COBEM 2021 26th International Congress of Mechanical Engineering
November 22-26, 2021, Virtual Congress, Brazil

COB-2021-1607
CFD MESH TOPOLOGY STUDY OF A TRUSS GEOMETRY UNDER FORCED OSCILLATIONS

Gustavo de Goes Gomes
Fillipe Rocha Esteves
José Rodolfo Chreim
Eduardo Tadashi Katsuno
Igor Andrade Coutinho
Fundação de Apoio ao Instituto de Pesquisas Tecnológicas, FIPT, São Paulo/Brasil
gggomes@ipt.br; filliperocha@ipt.br; jrchreim@ipt.br; katsuno@ipt.br; igorandrade@ipt.br

Leonardo de Oliveira Carvalho
Petrobras, Rio de Janeiro/Brasil
leonardo.carvalho@petrobras.com.br

João Lucas Dozzi Dantas
Instituto de Pesquisas Tecnológicas, IPT, São Paulo/Brasil
jdantas@ipt.br

Abstract. *When it comes to numerical models based on the finite volume method, a technique used in many computational fluid dynamics (CFD) simulations, the numerical mesh adopted gains considerable importance for the result of the simulations. Refinements at certain points of the geometry, such as with the usage of prismatic layers to better capture the flow boundary layer, or in the numerical domain, such as with wake or jet regions, for example, can make the representation of the studied phenomenon more reliable. Using a more refined mesh has a significant relation with the final expected result, however, it also comes with the trade-off of a higher computational cost. This paper seeks to demonstrate and evaluate a method to improve mesh topology based on the quantity of elements, therefore related to its computational cost, and the final results of the simulation. For this, a truss geometry is evaluated under the condition of forced oscillation, and its hydrodynamic coefficients of added mass and drag are measured. For a specific oscillation condition, a study is made with three different mesh topologies in which the vortices formed from the movement are evaluated. In these cases, the mesh verification process is also presented in order to establish the numerical uncertainties associated with each of them. The forces acting on the simulated body are obtained numerically using a commercial CFD software, and the hydrodynamic coefficients are calculated using the Morison model with the least squares method.*

Keywords: *Hydrodynamic Coefficients, CFD, Mesh Topology, Forced Oscillations.*

1. INTRODUCTION

Computational fluid dynamics (CFD) which relays over the finite volume method require the use of elements to fill a volume of interest in order to simulate its fluid flow. These elements constitute a mesh, which discretizes the volume of interest into control volumes, or areas for two dimensional cases, and flow equations are solved inside of it.(Lintermann, 2021) (Versteeg and Malalasekera, 2007). Their solution gives as a result the flow field for velocity, pressure, temperature, among others. Unfortunately, mesh generation is not a straightforward process, and a high quality mesh is not only important in order to obtain a reliable solution, but also to guarantee numerical stability. (Lintermann, 2021)

According to Versteeg and Malalasekera (2007), the accuracy of a CFD solution is directly linked to the number of cells in the mesh, usually, the larger, the better the solution accuracy. The problem with that is larger meshes are more costly, demanding more memory consumption and time, in order to solve all the required equations in every mesh cell.

Commonly, meshes can be divided in two major groups: structured and unstructured. This paper focus on the second, due to its advantages for simulations with complex geometries. Generating structured meshes for such geometries can be time consuming and require significant user intervention. (Ali *et al.*, 2017) (Lintermann, 2021). According to Lintermann (2021) unstructured CFD meshing technologies have matured and their usage has become more prevalent with commercial CFD softwares, providing simpler automated methods to achieve a meshed model.

Another advantage of unstructured meshes is that it is easier to do mesh refinements and adaption in comparison with the structured ones, since better meshes are often non-uniform: finer in areas with larger variations and coarser

in regions with little change, this type of mesh can be easily concentrated where necessary without wasting computer storage. (Versteeg and Malalasekera, 2007). In other words, it is possible to achieve representative results with a high quality mesh, without requiring excessive computational effort.

This paper presents a sequence from previous works related to CFD simulations for bodies under forced oscillation. In such works, there was an increase in the complexity of both model and studied bodies. In this paper, there is a further increase in the complexity of the body, and the focus is given to the study of mesh topology and refinement, since the results acquired employing the same method as before resulted in imprecise coefficients.

This paper is part of a larger project related to the estimation of the hydrodynamic coefficients, added mass, C_a, and drag, C_d, of equipment for the offshore industry. The increment in complexity, as mentioned before, is being made to increasingly mimic the geometries of equipment used in industry. The adoption of forced oscillation in the model is done in order to emulate the auxiliary ship motion in the process of installation equipment on the sea floor. As it is a process with many risks and high costs involved, it is important to have accurate knowledge on the coefficients of the pay-load, since its overestimation can lead to larger and more expensive crane vessels, whereas its underestimation can contribute to unsafe operations and an increase in the risk of accidents. (Mentzoni *et al.*, 2018)

2. PREVIOUS AND CURRENT WORK

In previous works (Gomes *et al.*, 2019) and (Gomes *et al.*, 2020), simulations were done over disks (both 2D and 3D) and 3D flat plates. The results were in good agreement with the ones presented by Tao and Dray (2008) and Tian *et al.* (2016), mainly for Keulegan-Carpenter, KC, numbers over 0.5. In these works, the major interest was in the determination of a model capable of representing the fluid flow and the resulting forces from the body movement in order to obtain the hydrodynamic coefficients of interest. Figures 1 and 2 present the added mass and drag coefficient results for the disks in comparison with the cited authors.

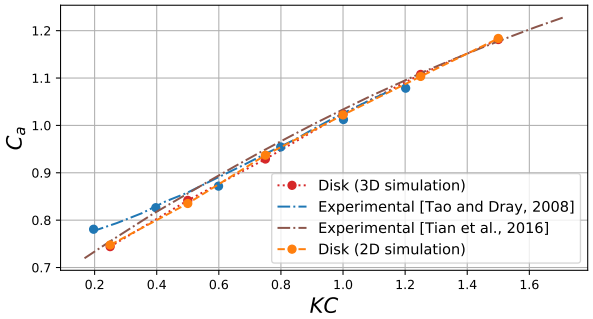

Figure 1. Added mass coefficient for a disk (Gomes *et al.*, 2020)

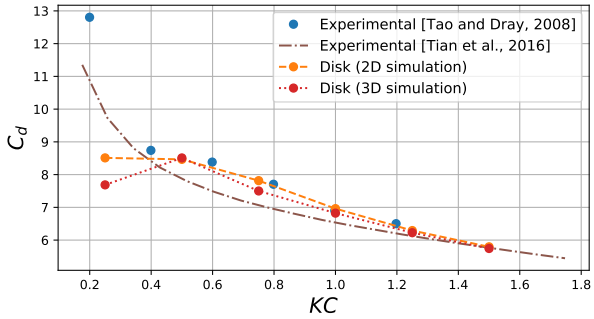

Figure 2. Drag coefficient for a disk (Gomes *et al.*, 2020)

From the figures it is possible to infer that the results are in good agreement with the ones presented in the literature, the main differences are related to C_d for low KC values.

In this paper, the interest is to represent a more complex geometry using unstructured three-dimensional mesh with the model proposed in the previous works. Initially, a mesh built in the same way as before was used, from its results and the solution verification analysis two new mesh topologies are proposed in order not only to improve its outcome, but also to reduce mesh uncertainty and computational cost of each simulation.

3. NUMERICAL MODEL

This section presents a brief summary of the model created previously. In the model it is imposed a sinusoidal motion on the equipment given by Eq. (1).

$$S(t) = A\cos(\omega t) \tag{1}$$

In which A is the amplitude and ω is the circular frequency of the movement. There are two important dimensionless numbers for bluff bodies under this kind of motion, these are the Keulegan-Carpenter number, KC, and β (Sarpkaya, 2010), presented in Eq. (2).

$$KC = \frac{2\pi A}{L} \qquad \beta = \frac{L^2}{\nu T} = \frac{Re}{KC} \tag{2}$$

In which L is a characteristic length of the body, ν is the kinematic viscosity of the fluid, T is the oscillation period and Re is the Reynolds number of the flow. This Re is calculated based on the highest velocity experienced by the body under oscillation.

Even though the geometry of interest is different from disks and flat plates, the same conclusions from Tao and Dray (2008), Li *et al.* (2013) and Mentzoni *et al.* (2018) are adopted, that there is a weak relation between the frequency of oscillation and the hydrodynamic coefficients for low KC numbers, in other words, changes in β do not result in significant changes in the hydrodynamic coefficients. So, only the value of 2.24 s was used for the T in the simulations.

As before, the software ANSYS Fluent, 2020 R2, double precision, was used. The fluid adopted was liquid water with constant density, and the oscillation movement was done over the entire domain employing a reference frame motion. By doing it this way, there is a simplification in the problem, avoiding mesh changes throughout the simulation. (Dütsch *et al.*, 1997).

The motion of the domain is set by a user-defined function according to a velocity input, which is set based on the derivative of Eq. (1), presented by Eq. (3).

$$\dot{S}(t) = -A\omega \sin(\omega t) \tag{3}$$

It is important to notice that the same geometry, with the same L, was used in all simulation cases. Thus, a change in KC affect only the A, changing also the motion velocity. The time step of the simulations was set as T/1600.

The turbulence model $k - k_l - \omega$ was used again, due to its capability of simulating the transition between laminar and turbulent regimes and good agreement achieved with experimental data presented in the previous works.

The hydrodynamic coefficient calculation used the least squares method, as presented in Journée and Massie (2001). In which the Morison equation, Eq. (4), is computationally approximated with the measured force by correcting the values of C_a and C_d, according to the acceleration and velocity of the body. In this formulation, both coefficients are assumed to be independent.

$$F = \rho\, C_a\, \nabla\, \ddot{S}(t) + \frac{1}{2}\, \rho\, C_d\, A_p\, |\dot{S}(t)|\, \dot{S}(t) \tag{4}$$

In Eq. (4), ρ is the fluid density; ∇, the volume; A_p, the front area; $\ddot{S}(t)$, the acceleration, and $\dot{S}(t)$, the velocity of the body. More information on the model and numerical method can be seen in the previous works and in Chreim *et al.* (2020).

4. STUDY CASE

For the study case presented in this paper, it was chosen a truss geometry, shown in Fig. 3 along with the adopted Cartesian coordinate system. The body is composed of thirteen squared bars with cross-section of 15 mm, and its main dimensions are presented in Tab. 1. This geometry was chosen due to available experimental data and the subtle increase in geometry complexity.

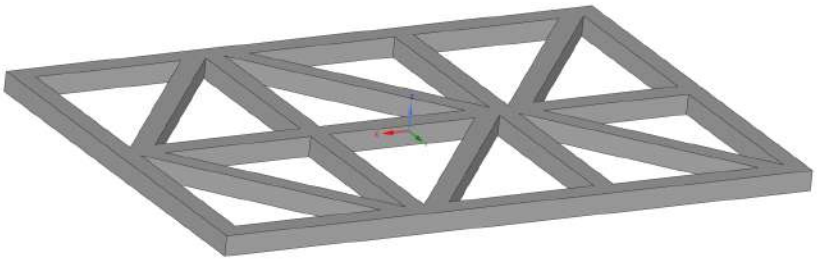

Figure 3. Study case geometry

Table 1. Characteristics of the study case geometry

Dim. X [mm]	**Dim. Y [mm]**	**Dim. Z [mm]**	**Projected Area A_p [m^2]**
465	315	15	0.053

For the construction of the fluid domain, the largest dimensions of the body were used, in order to guarantee sufficient distance to the (external) domain. Thus, a domain equal to 7.5$\times$ the largest geometry dimension in each direction was used. (Gomes *et al.*, 2020). A Y normal symmetry plane was adopted, in order to reduce the total amount of elements in the mesh. In the Z direction, parallel to the oscillatory movement, it was employed 7.5$\times$ the largest transverse dimension of the geometry, 465 mm, for both positive and negative Z.

Within the domain, two 'Body of Influence' type refining regions were created using the Ansys Fluent mesh generator: one called Refinement B, close to the vortex shedding region, with smaller dimensions and smaller characteristic

elements – equal to five percent of the maximum dimension established at the domain boundaries – and another, exterior, surrounding both the geometry and Refinement B, called Refinement A, with elements twice the size of B. Refinement B consists of a box with rounded edges and vertices so as to enclose the geometry of interest.

Six prismatic layer elements were used, with the height of the closest to the wall equal to 0.035 mm, in order to achieve y^+ below 1 in most of the simulation for all cases. The mesh topology was the poly-hexcore, which employs hexahedral elements in most of the fluid domain and for the union with the prismatic elements, polyhedral elements are used. Figure 4 shows the created mesh, where it is possible to see both refinement regions, Tab. 2 presents the characteristic sizes for each region of the domain, alongside with its total number of elements.

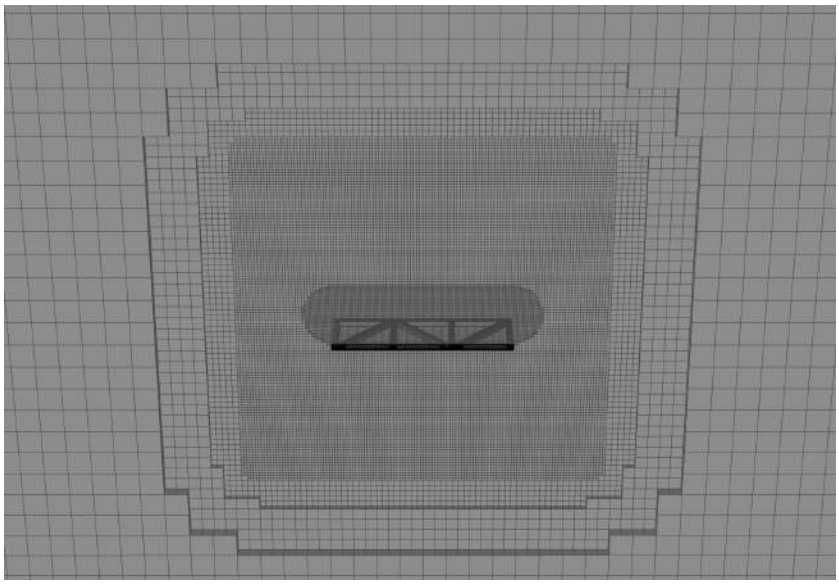

Figure 4. Study case mesh 1

Table 2. Characteristics of the first created mesh

Max. element dimension [mm]	**Refinement A [mm]**	**Refinement B [mm]**	**Total n^o of elements (x10^3)**
80	8	4	1204.25

For this first mesh, 10 values of KC were simulated, between 0.15 and 3.00, using the same value of 2.24 s for the oscillation period.

4.1 Initial results and solution verification analysis

Figure 5 shows the results for C_d in comparison with experimental data using the model presented before.

From the figure, it is possible to see that there is better agreement between the numerical and experimental data mainly for the lowest values of KC for one of the datasets. However, for higher KC values there is a notable difference in the results, with the numerical data being higher than the experimental. Due to the results, and to grasp more knowledge on possible errors of the simulated model, it was decided to carry-out a solution verification analysis.

This analysis was based on the work of Eça and Hoekstra (2014) and was performed using the Numerical Uncertainty Analysis (NUA) software. The adopted method to estimate the uncertainty uses an integral or local result from the simulation, and requires a series of geometrically similar meshes with a systematic refinement between each one of them.

In this case, the discretization error ϵ_ϕ, related to the mesh, was estimated from power series expansions as a function of the refinement ratio between each mesh.

According to the authors, ϵ_ϕ usually is dominant in this kind of numerical simulation and can be a consequence, for example, of the discretization method used, due to the approximations made to transform the differential equations that govern the problem into a system of algebraic equations. As the numerical mesh becomes more refined, this type of error tends to decrease. Other errors presented in these kind of simulation are related to round-off and iteration. The former is a consequence of the finite precision of computers, and can be significantly reduced using double precision in the software. The second is a consequence of the non-linearity of the equations, and can be reduced by employing a higher number of intermediate iterations between each time-step. Since the simulations are unsteady, there is also the statistical error related to the calculated force from each cycle of oscillation in the simulation. In order to decrease this error, only data from the last cycles were used to calculate the hydrodynamic coefficients, so the initial transient regime had a diminished influence

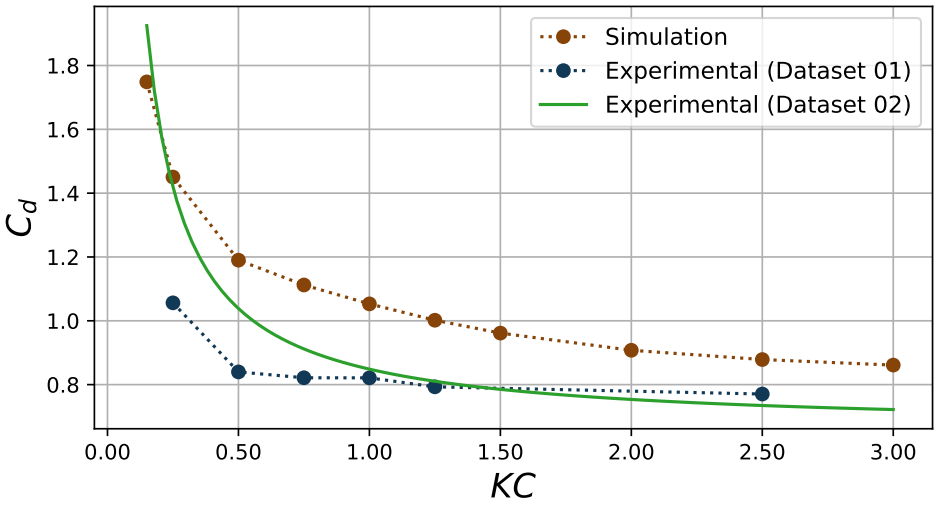

Figure 5. Drag coefficient results

on the results. In this work, the last three errors were considered less relevant than the discretization for the simulations performed.

After the calculation of the discretization error, the uncertainty U_ϕ of the solution is estimated with a 95% confidence interval. More details on the calculations of ϵ_ϕ and U_ϕ are presented in Eça and Hoekstra (2014).

The solution verification analysis was carried out to obtain the numerical uncertainty of the simulations and give better credibility to the outcome obtained. For this, the results of the hydrodynamic coefficients C_a and C_d for six topologically similar meshes were analyzed. The meshes were created based on the one presented in the previous section by progressively reducing or increasing the size of its elements by $\sqrt{2}$. Three finer and two coarser meshes were created, thus, a total of six meshes were analysed. As it is a highly computational cost analysis, it was performed only for the value of KC equal to 1.00.

In order to identify the meshes, a new nomenclature had to be used, in which the base mesh is called VVM0, the coarser meshes, VVM-, and VVM2-, the last being the least refined among all those created. For the more refined ones, the plus symbol is used, and these are called VVM+, VVM2+ and VVM3+, where the latter was the most refined mesh in the study. Table 3 presents the refinement ratio, or relative step size, and the amount of elements for each mesh.

Table 3. Characteristics of the solution verification meshes

	VVM2-	**VVM-**	**VVM0**	**VVM+**	**VVM2+**	**VVM3+**
Relative step size	$4\sqrt{2}$	4	$2\sqrt{2}$	2	$\sqrt{2}$	1
Number of elements (10^3)	205.8	472.2	1204.2	3001.9	7819.4	20786.4

Since the hydrodynamic coefficients are being used as the numerical quantity from the simulations to calculate the uncertainties, inevitably there is a combined error between mesh and method of analysis. As the method adopted is the same in all cases, it was assumed that the relative error is always the same.

Even though the simulations are unsteady, there has not been an in-depth study in relation to temporal discretization. Therefore, it was only chosen to investigate the mesh, or spatial, discretization error. Figures 6 and 7 present the uncertainty results for C_a and C_d, respectively.

From the figures, there is better convergence for the values of C_d in relation to those of C_a. Actually, the value of U_ϕ for C_a is excessive, and the observed order of precision, p, is in the empirically acceptable lower limit, according to Eça and Hoekstra (2014), which can make the uncertainty estimate too conservative.

In order to improve the results obtained, related to both numerical uncertainty and drag coefficients in comparison with the experimental data, it was decided to carry out a new study, in this case, related to mesh topology.

4.2 Mesh topology study

For the mesh topology study, the flow results from the previous simulations were analyzed. This analysis was based on the vorticity field in a Y-plane that passes through the structure, as shown in Fig. 8.

This initial analysis is important to investigate the regions of major interest to be further refined, and thus propose new mesh topologies that can better capture both the forces generated by the movement and the resulting vortices. For this, the

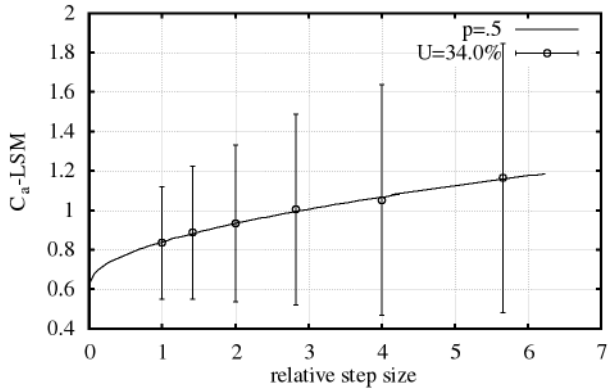

Figure 6. Solution verification result for the added mass coefficient

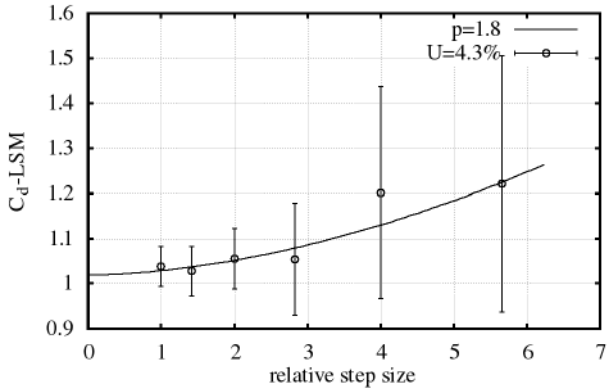

Figure 7. Solution verification result for the drag coefficient

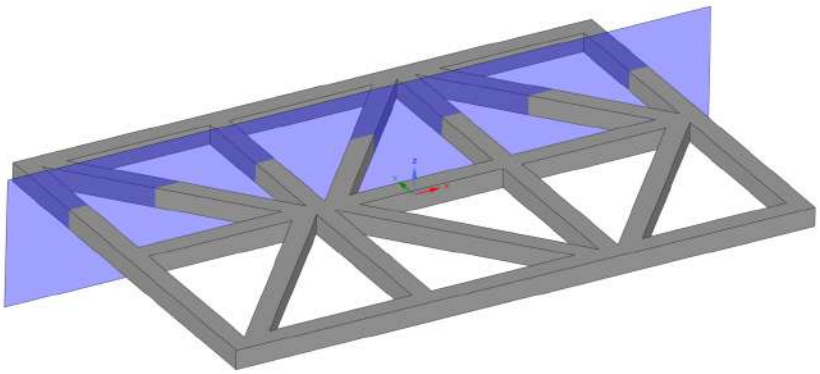

Figure 8. Plane location for the vorticity field study

vorticity field results of the previous simulations were used, with KC = 1.00, and it was established an absolute vorticity value of 5 s^{-1} as basis for comparison between the simulations. This value was chosen, because it delimits the higher vorticity intensity near the bars from the rest of the simulation domain. For this analysis, only the first 3 squared bars of the structure, from left to right, were selected and numbered in the same order.

Figures 9, 10 and 11 show the vorticity field in the chosen plane at the moment of the highest movement speed for the meshes VVM2-, VVM0 and VVM3+, respectively. It is important to mention that the analysis also took into account the vorticity field at the instant of lowest speed.

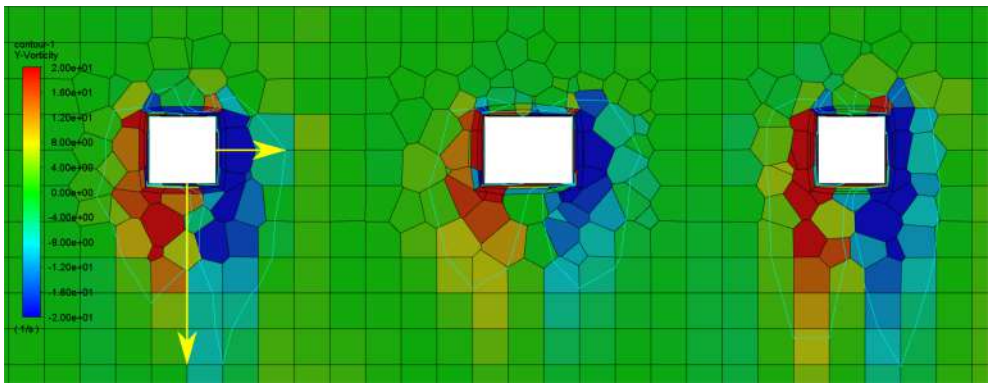

Figure 9. Vorticity field result (mesh VVM2-)

From the figures, the representation of the vortices is better, and more easily identified, as the mesh becomes more refined. The figures also represent, by a thin line in light blue, the flow regions that have an absolute value for vorticity of 5 s^{-1}. Only Fig. 9 shows the directions from which the distance between the squared bars and the vortex extremity were measured. Its objective is to establish a more suitable size for the refinement region to be used in the new mesh topologies.

Table 4 presents the results of this process for the selected flows, in which it shows both the values for the distance in relation to the squared bars in the vertical direction, parallel to the flow, and the results in the horizontal direction, perpendicular to the flow.

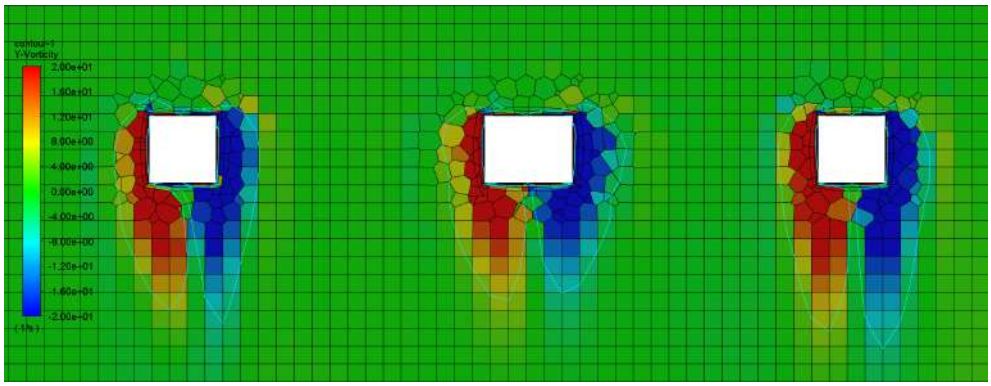

Figure 10. Vorticity field result (mesh VVM0)

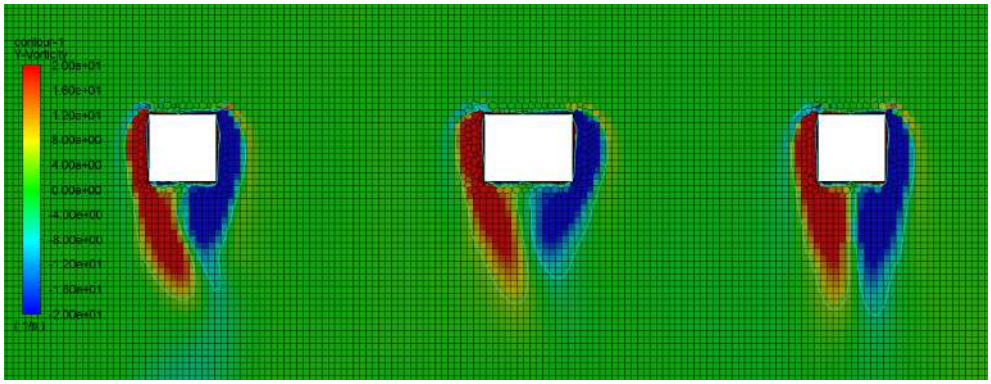

Figure 11. Vorticity field result (mesh VVM3+)

Table 4. Size between the squared bars and vorticy equal to $\pm$ 5 s^{-1}. Units in [mm]

	Vertical direction						Horizontal direction					
	Maximum Velocity			Minimum Velocity			Maximum Velocity			Minimum Velocity		
	Bar 1	**Bar 2**	**Bar 3**	**Bar 1**	**Bar 2**	**Bar 3**	**Bar 1**	**Bar 2**	**Bar 3**	**Bar 1**	**Bar 2**	**Bar 3**
VVM2-	40.00	32.00	40.00	32.00	8.00	4.00	16.00	16.00	16.00	16.00	16.00	16.00
VVM-	50.91	28.28	39.60	33.94	16.97	19.80	16.97	16.97	11.31	16.97	16.97	11.31
VVM0	36.00	28.00	**40.00**	20.00	10.00	14.00	12.00	16.00	12.00	16.00	16.00	12.00
VVM+	28.28	25.46	33.94	16.97	8.49	14.14	8.49	11.31	8.49	14.14	14.14	11.31
VVM2+	30.00	26.00	32.00	18.00	10.00	16.00	8.00	10.00	8.00	16.00	16.00	14.00
VVM3+	26.87	28.28	29.70	22.63	9.90	16.97	7.07	8.49	7.07	**18.36**	14.14	14.14

From the table, it is possible to see the distance necessary for the representation of each of the vortices of interest, obviously, according to the metric that its extremity has an absolute vorticity value of 5 s^{-1}. Therefore, it was decided to adopt the values of 40 mm parallel, and 20 mm perpendicular to the flow. These sizes were the basis for the new refinements used in the construction of two distinct, but similar, mesh topologies.

4.3 New mesh topologies

The new topologies were built from the same refining bodies used before, but with the addition of two new ones inside Refiniment B. Figures 12 and 13 show the refining bodies created for the two topologies, named domain 2 and 3, respectively. In the figures, the refinement B is represented in orange, and in green and blue the two new refinements. The green one is common to both domains and is formed by oval cylinders that cover the structure, with the smaller radius with 37.5 mm, and the larger with 62.5 mm. The refinements in blue are different, in domain 2 it is composed of cylinders with a radius of 18.75 mm, while in domain 3 it is made of oval cylinders with smaller radius of 27.5 mm and larger of 47.5 mm, which has the values obtained in the previous section. Regarding domain 2, the region in green is responsible for the vortex characterization, since the refinement in blue is smaller, therefore, being more linked to the vortex formation.

The size of the elements used in each region were the same as previously adopted for refinements A and B, as shown in Tab. 5, in which the refinements in green and blue are called C and D, respectively.

From Tab. 5, it is possible to see that the amount of elements in domain 3 is almost two times higher than domain

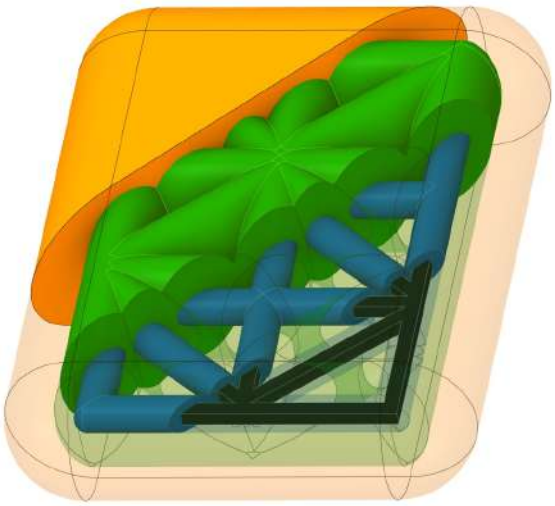

Figure 12. Domain 2 - refinement bodies

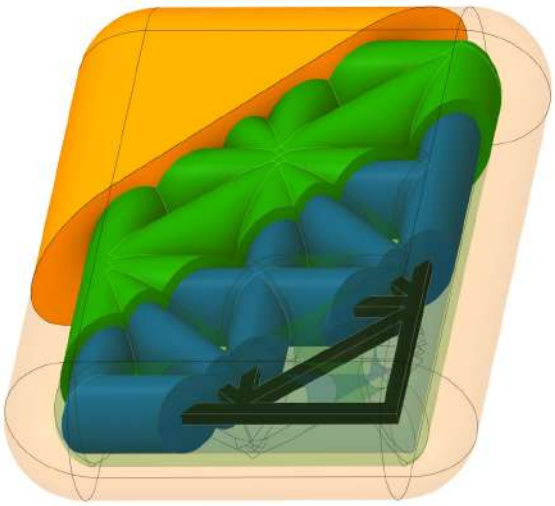

Figure 13. Domain 3 - refinement bodies

Table 5. Characteristics of the new meshes

Domain	**Max. dim. [mm]**	**Ref. A [mm]**	**Ref. B [mm]**	**Ref. C [mm]**	**Ref. D [mm]**	**N^o elements (x10^6)**
VVM0 (1)	80	8	4	-	-	1.20
VVM3+ (1)	$20\sqrt{2}$	$2\sqrt{2}$	$\sqrt{2}$	-	-	20.79
2	80	8	4	2	1	5.21
3	80	8	4	2	1	9.58

2, because of the larger Refinement D region. In addition, it is important to note that the value used for the elements of Refinement D is smaller than the refinement B of VVM3+ mesh, which has 20.8 million elements, nearly two times the number of elements of domain 3. Figures 14 and 15 present the meshes of domain 2 and 3, where it is easier to see the differences in the adopted topologies.

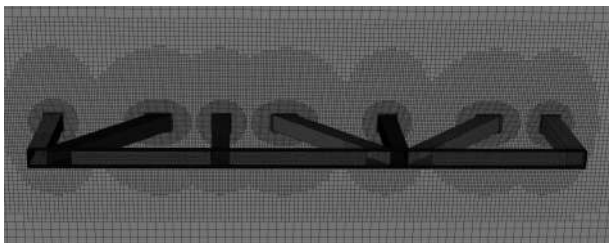

Figure 14. Domain 2 - Mesh detail

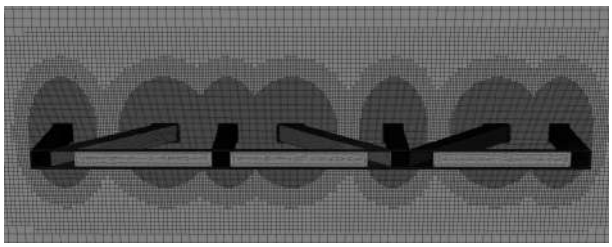

Figure 15. Domain 3 - Mesh detail

4.4 Result comparison

With the two new meshes, a new verification process was carried out, but this time using only 3 levels of refinement for each of the new topologies, due to the high cost of this kind of analysis. The meshes presented in Tab. 5 were the base mesh for the process, and for each of them, a more and a less refined one was created with a refining ratio of $\sqrt{2}$. Figures 16 to 19 show the results for the uncertainty of the added mass and drag coefficient solutions for both domains.

From the figures, it is possible to see that there is a significant improvement in the convergence of the added mass coefficient, with an uncertainty value going from 34% for the VVM3+ mesh of the previous case (Fig. 6) to 2.4% for domain 2 (Fig. 16). The drag coefficient, on the other hand, maintains almost the same value for all the studied cases, but there is an inversion in the concavity of the curve.

As it is assumed that the error related to discretization is dominant in relation to round-off, iteration and statistical, it can be said that there was a significant reduction in the error of the simulations, due to the change in the topologies, and consequently, the uncertainty in relation to its results were also reduced.

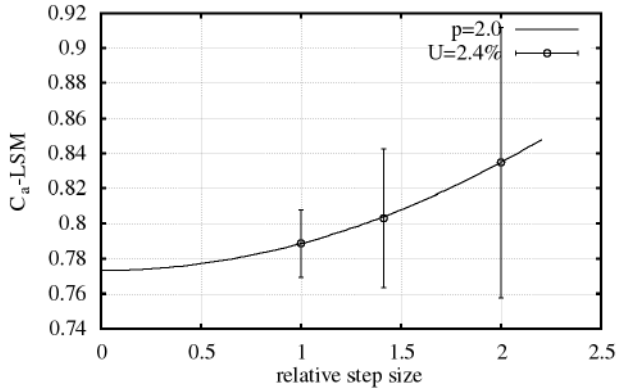

Figure 16. Solution verification result for the added mass coefficient (Domain 2)

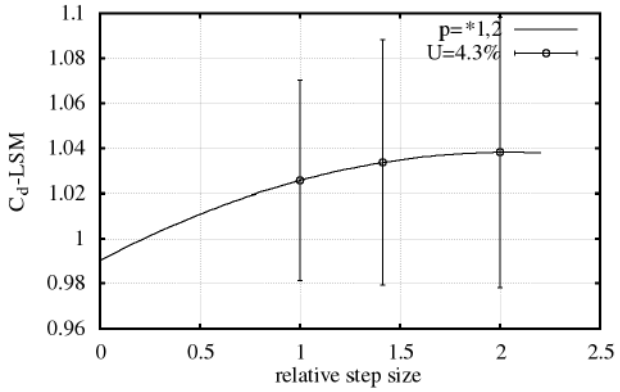

Figure 17. Solution verification result for the drag coefficient (Domain 2)

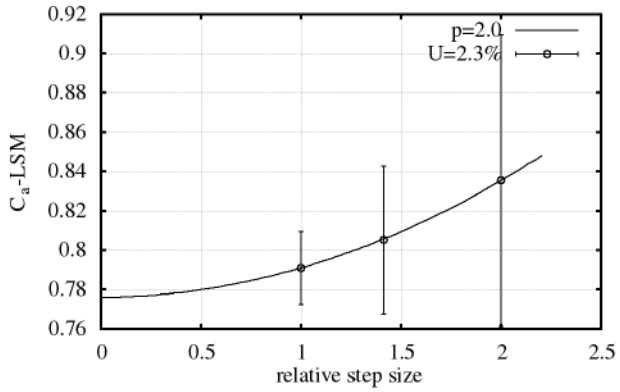

Figure 18. Solution verification result for the added mass coefficient (Domain 3)

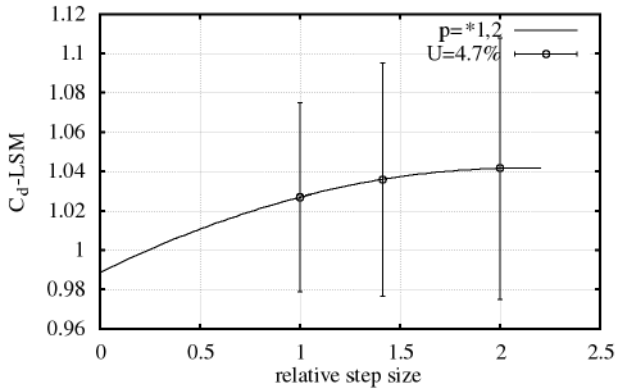

Figure 19. Solution verification result for the drag coefficient (Domain 3)

In order to better analyze the efficiency of each mesh topology, a comparison between the coefficients obtained for each simulation as a function of the number of mesh elements is presented in Fig. 20, for C_a, and in Fig. 21, for C_d, the error bars represent the calculated numerical uncertainty of the simulations.

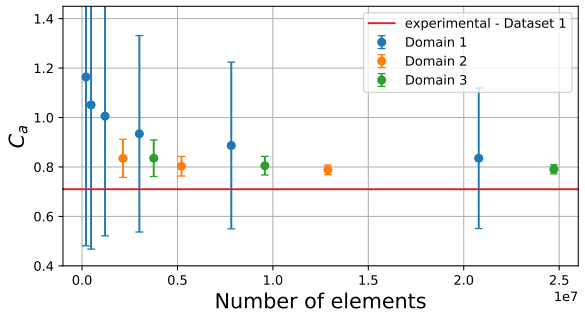

Figure 20. Refinement level comparison for the added mass coefficient (KC = 1,00)

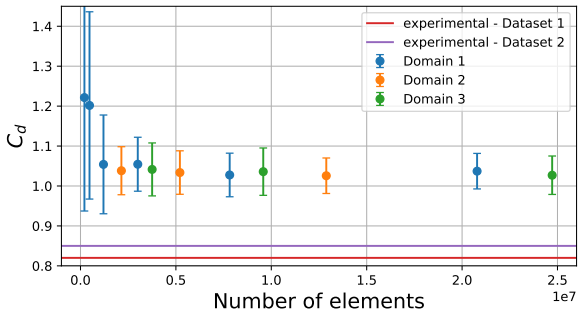

Figure 21. Refinement level comparison for the drag coefficient (KC = 1,00)

From the figures, excluding the two less refined meshes from domain 1, as the number of elements increases the drag coefficient does not change much. Regarding the added mass coefficient, it is noted that the mesh refinement for domain 1 generates a significant change in the coefficient, whereas for the other two, this difference is only noticeable for the less refined meshes. Furthermore, comparing the results of the finer mesh in domain 1, VVM3+, with the results of the other domains there is little difference in the coefficient values and, in most cases, a significant reduction in the number of elements and in the uncertainty of the simulation. Thus, it can be concluded that both domains 2 and 3 present results similar to those of the initial domain with a high level of refinement, requiring lower computational cost, and with a numerical uncertainty value significantly lower. However, there are still differences in relation to the experimental results, around 10% for C_a and 20% for C_d.

5. CONCLUSION

This paper presented a study related to mesh topology and refinement of CFD simulations, which is part of a bigger research related to the calculation of hydrodynamic coefficients of subsea structures. From the employed method, based on the resultant flow characteristics, one can conclude that in the new mesh topologies there was a reduction of both computational cost and numerical uncertainty, with a similar final coefficient result, when comparing with the most refined mesh from the first mesh topology. Specific for the study case presented, if more focus is given to the value of the obtained coefficients, domain 2 may be a better choice, because of its analogous results and lower computational cost. Whereas, if more focus is given to the resultant flow topology, domain 3 may be recommendable, since it has a higher number of elements with small size near the geometry. In future stages, it is intended to estimate the uncertainty related to both spatial and temporal discretization of the simulations with the three different domains, in order to have a better picture of its most relevant uncertainties. Besides that, it will be interesting to simulate using the presented method, more realistic geometries, which are representative of equipment used in the offshore industry.

6. ACKNOWLEDGMENTS

The authors would like to thank the Petróleo Brasileiro SA (Petrobras) for the funding and scholarship support through the Research and Development fund (5900.0113197.19.9) of the Agência Nacional do Petróleo, Gás Natural e Biocombustíveis (ANP); and the funding from FINEP (agreement 01.18.0082.00 - CTInfra 2014) and Fapesp (PDIP Process 2017/50343-2).

7. REFERENCES

Ali, Z., Tucker, P.G. and Shahpar, S., 2017. "Optimal mesh topology generation for cfd". *Computer Methods in Applied Mechanics and Engineering*, Vol. 315, pp. 431–457.

Chreim, J.R., Esteves, F.R., Gomes, G.G., Carvalho, L.O. and Dantas, J.D., 2020. "A study on the several methods for the calculation of the hydrodynamic coefficients in forced oscillation experiments". In *28th International Congress on Waterborne Transportation, Shipbuilding and Offshore Constructions Proceedings - SOBENA 2020*. Rio de Janeiro, RJ, Brazil.

Dütsch, H., Durst, F., Becker, S. and Lienhart, H., 1997. "Low-reynolds-number flow around an oscillating circular cylinder at low keulegan-carpenter numbers". *Journal of Fluid Mechanics*, Vol. 360, p. 249 – 271.

Eça, L. and Hoekstra, M., 2014. "A procedure for the estimation of the numerical uncertainty of cfd calculations based on grid refinement studies". *Journal of Computational Physics*, Vol. 262, p. 104 – 130.

Gomes, G.G., Dantas, J.D. and Assi, G.S., 2019. "Numerical study of flow around oscillating simple geometries using porous medium". In *25th ABCM International Congress of Mechanical Engineering - COBEM 2019*. Uberlândia, MG, Brazil.

Gomes, G.G., Esteves, F.R., Chreim, J.R., Carvalho, L.O. and Dantas, J.D., 2020. "Numerical study of the hydrodynamic coefficients of simple geometries under forced oscillations". In *28th International Congress on Waterborne Transportation, Shipbuilding and Offshore Constructions Proceedings - SOBENA 2020*. Rio de Janeiro, RJ, Brazil.

Journée, J.M. and Massie, W.W., 2001. *Offshore Hydromechanics*. Delft University of Technology, Delft, Netherlands.

Li, J., Liu, S., Zhao, M. and Teng, B., 2013. "Experimental investigation of the hydrodynamic characteristics of heave plates using forced oscillation". *Ocean Engineering*, Vol. 66, p. 82 – 91.

Lintermann, A., 2021. *Clinical and Biomedical Engineering in the Human Nose - A Computational Fluid Dynamics Approach - Chapter 6. Computational Meshing for CFD Simulations*. Springer Singapore, Singapore.

Mentzoni, F., Abrahamsen-Prsic, M. and Kristiansen, T., 2018. "Hydrodynamic coefficients of simplified subsea structures". In *Proceedings of the ASME 2018 37th International Conference on Ocean, Offshore and Arctic Engineering - OMAE 2018*. Madrid, Spain.

Sarpkaya, T., 2010. *Wave Forces on Offshore Structures*. Cambridge University Press, Cambridge, England.

Tao, L. and Dray, D., 2008. "Hydrodynamic performance of solid and porous heave plates". *Ocean Engineering*, Vol. 35, p. 1006 – 1014.

Tian, X., Li, X. and Yang, J., 2016. "Hydrodynamic coefficients of oscillating flat plates at $0.15 \leq \text{kc} \leq 3.15$". *Journal of Marine Science and Technology*, Vol. 22, p. 101 – 113.

Versteeg, H.K. and Malalasekera, W., 2007. *An Introduction to Computational Fluid Dynamics - The Finite Volume Method*. Pearson Education Limited, Harlow, England.

8. RESPONSIBILITY NOTICE

The authors are solely responsible for the printed material included in this paper.